Dalton Transactions

ROYAL SOCIETY OF CHEMISTRY

PAPER

View Article Online
View Journal | View Issue

Check for updates

Cite this: *Dalton Trans.*, 2021, **50**, 8549

Synthesis, structure, and photoluminescence of the chloridoaluminates [BMIm][Sn(AlCl$_4$)$_3$], [BMPyr][Sn(AlCl$_4$)$_3$], and [BMIm][Pb(AlCl$_4$)$_3$]†

Silke Wolf, Mareike Liebertseder and Claus Feldmann *

Received 2nd November 2020,
Accepted 27th May 2021

DOI: 10.1039/d0dt03766d

rsc.li/dalton

[BMIm][Sn(AlCl$_4$)$_3$] (**1**) ([BMIm]: 1-butyl-3-methylimidazolium), [BMPyr][Sn(AlCl$_4$)$_3$] (**2**) ([BMPyr]: 1-butyl-1-methyl-pyrrolidinium), and [BMIm][Pb(AlCl$_4$)$_3$] (**3**) are obtained by reaction of SnCl$_2$/PbCl$_2$ in [BMIm]Cl/[BMPyr]Cl/AlCl$_3$-based ionic liquids. The colourless crystals of the title compounds contain infinite $^1_\infty$[M(AlCl$_4$)$_3$]$^{n-}$ chains (M: Sn, Pb) that are separated by the voluminous [BMIm]$^+$/[BMPyr]$^+$ cations. The central Sn^{2+}/Pb^{2+} is coordinated by chlorine in the form of distorted squared anti-prismatic polyhedra. Each Cl atom, in turn, is part of an [AlCl$_4$]$^-$ tetrahedron that interlinks Sn^{2+}/Pb^{2+} to the chain-like building unit. In addition to the novel structural arrangement, all title compounds surprisingly show intense white-light emission. Although Sn^{2+} and Pb^{2+} are well-known as dopants in conventional phosphors, efficient luminescence *via* s–p-transitions of compounds containing Sn^{2+}/Pb^{2+} in molar quantities and as regular lattice constituents is rare. The emission of [BMIm][Sn(AlCl$_4$)$_3$] and [BMPyr][Sn(AlCl$_4$)$_3$] is very efficient with quantum yields of 51 and 76%, which belong to the highest values known for s–p-based luminescence of Sn^{2+}.

Introduction

The synthesis of complex metal halides was most often performed in solution or *via* solid-state reactions.[1] Usually the dissolution of a metal halide requires the coordination of the metal cation by the respective solvent and often results in coordination compounds with solvent molecules serving as ligands being part of the composition of the complex metal halide.[1] Solid-state reactions require high temperatures (typically >300 °C) to guarantee sufficiently fast diffusion in the solid state.[1] On the other hand, high temperatures are counterproductive when aiming at kinetically stabilized and thermodynamically metastable compounds. Since activation barriers can be passed, only the thermodynamically most stable compound might be obtained at high temperatures.[2] Another difficulty relates to the sensitivity of many metal halides to hydrolysis, which is all the higher the more Lewis-acidic and the higher the charge density of the respective metal cations is. Besides long-known molten salts (*e.g.* LiCl/KCl mixtures),[1,3] ionic liquids turned out as versatile media that combine both the absence of (strongly) coordinating ligands and a good solubility of many metal halides.[4] Especially, Lewis-acidic ionic liquids – most often AlCl$_3$-based systems – have already shown great potential to realize new compounds that can be hardly prepared in other solvents.[5] Some recent examples include, for instance, the intermetalloid [CuBi$_8$]$^{3+}$ cluster cation in [CuBi$_8$][AlCl$_4$]$_2$[Al$_2$Cl$_7$],[6] the Ge$_{12}$Fe$_8$ cluster core in Ge$_{12}$(μ-I)$_4${Fe(CO)$_3$}$_8$,[7] the [Sb$_{10}$Se$_{10}$]$^{2+}$ cation in [Sb$_{10}$Se$_{10}$][AlCl$_4$]$_2$,[8] the clathrate phases K$_x$Ge$_{136}$ or Na$_x$Si$_{136}$,[9] the direct-gap semiconductor [Bi$_2$Te$_2$Br][AlCl$_4$],[10] or the hexanuclear Zr$_6$ cluster in Zr$_6$Br$_{14}$Fe or Li$_2$Zr$_6$Cl$_{15}$Mn.[11]

By reaction of SnCl$_2$/PbCl$_2$ in [BMIm]Cl/[BMPyr]Cl/AlCl$_3$-based ionic liquids, we could now prepare the chloridoaluminates [BMIm][Sn(AlCl$_4$)$_3$] (**1**), [BMPyr][Sn(AlCl$_4$)$_3$] (**2**), and [BMIm][Pb(AlCl$_4$)$_3$] (**3**) ([BMIm]: 1-butyl-3-methylimidazolium), ([BMPyr]: 1-butyl-1-methyl-pyrrolidinium). Besides new structural features, the compounds surprisingly show intense s–p-based photoluminescence although luminescence quenching is usually expected for high concentrations of the luminescent centers in the host lattice.

Results and discussion

Ionic-liquid-based synthesis

[BMIm][Sn(AlCl$_4$)$_3$] (**1**), [BMPyr][Sn(AlCl$_4$)$_3$] (**2**), and [BMIm][Pb(AlCl$_4$)$_3$] (**3**) were prepared by reaction of the respective divalent chlorides SnCl$_2$ and PbCl$_2$ in an ionic liquid established by a mixture of [BMIm]Cl or [BMPyr]Cl and AlCl$_3$ with a ratio of

Institut für Anorganische Chemie, Karlsruhe Institute of Technology (KIT), Engesserstrasse 15, D-76131 Karlsruhe, Germany. E-mail: claus.feldmann@kit.edu; Fax: +49 721 608 47021; Tel: +49 721608 42855, +49 721 608 42856, http://www.kit.edu

† Electronic supplementary information (ESI) available. CCDC 2041327–2041329. For ESI and crystallographic data in CIF or other electronic format see DOI: 10.1039/d0dt03766d

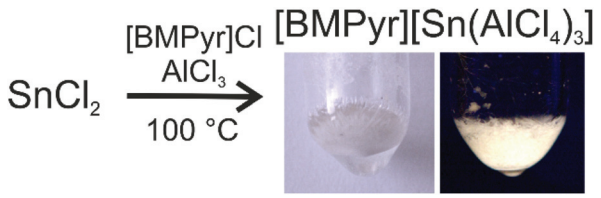

Fig. 1 Scheme to illustrate the synthesis approach with [BMPyr][Sn($AlCl_4$)$_3$] (**2**) as example.

1 : 3 (Fig. 1). All reactions were performed in sealed, Argon-filled glass ampoules by heating to 70–100 °C for 12 hours. The specific temperature is required to guarantee that the reaction mixture is completely liquid at the respective temperature as well as to promote the diffusion of the reactants and the formation of single crystals with suitable crystal quality. Whereas lower temperatures result in a lower yield and a poor crystal quality, higher temperatures lead to a decomposition of the ionic liquid. The formation of the title compounds can be rationalized based on the following reactions:

1:

$$SnCl_2 + [BMIm]Cl + 3AlCl_3 \rightarrow [BMIm][Sn(AlCl_4)_3]$$

2:

$$SnCl_2 + [BMPyr]Cl + 3AlCl_3 \rightarrow [BMPyr][Sn(AlCl_4)_3]$$

3:

$$PbCl_2 + [BMIm]Cl + 3AlCl_3 \rightarrow [BMIm][Pb(AlCl_4)_3]$$

The synthesis of the title compounds requires ionic liquids as the liquid phase. Specific advantages comprise the presence of voluminous cations, the Lewis acidity, the low melting point, the absence of any strong-coordinating solvent molecules, as well as the strict absence of moisture. In comparison to [BMIm]Cl/$AlCl_3$, the system [BMPyr]Cl/$AlCl_3$ results in significantly smaller crystallites. Such behaviour with the cation of the ionic liquid influencing the crystallization and crystal quality is often observed and can be ascribed to the volume of the one or other cation, which fits best with certain crystal structure.[4,12]

Structure and composition

All title compounds crystallize as colourless, slightly elongated plates with monoclinic lattice symmetry in the space group *C*2/*c* (Table 1). They consist of infinite $^1_\infty[M(AlCl_4)_3]^{n-}$ chains (M: Sn, Pb), which are separated by the voluminous $[BMIm]^+$/$[BMPyr]^+$ cations (Fig. 2; ESI: Fig. S1 and S2†). The latter naturally stem from the ionic liquid. The most interesting building unit in the title compounds relates to the $^1_\infty[M(AlCl_4)_3]^{n-}$ chains, which – to the best of our knowledge – have not been observed until now. In the anionic $^1_\infty[M(AlCl_4)_3]^{n-}$ chains, each Sn^{2+}/Pb^{2+} is surrounded by five $[AlCl_4]^-$ tetrahedra, resulting in

Table 1 Crystallographic and refinement details of [BMIm][Sn($AlCl_4$)$_3$] (**1**), [BMPyr][$SnCl_4$] (**2**), and [BMIm][Pb($AlCl_4$)$_3$] (**3**)

Data	1	2	3
Sum formula	$C_8H_{15}N_2Cl_{12}Al_3Sn$	$C_9H_{20}NCl_{12}Al_3Sn$	$C_8H_{15}N_2PbAl_3Cl_{12}$
Crystal system	Monoclinic	Monoclinic	Monoclinic
Space group	*C*2/*c*	*C*2/*c*	*C*2/*c*
Lattice parameters	a = 1506.3(3) pm b = 1556.9(2) pm c = 1198.6(2) pm β = 100.2(1)°	a = 1511.0(1) pm b = 1556.3(1) pm c = 1197.2(1) pm β = 96.5(1)°	a = 1506(1) pm b = 1553(1) pm c = 1188(1) pm β = 100.0(1)°
Cell volume	$V = 2766.5 \times 10^6$ pm^3	$V = 2797.1 \times 10^6$ pm^3	$V = 2735 \times 10^6$ pm^3
Formula units per cell	Z = 4	Z = 4	Z = 4
Calculated density	ρ = 1.835 g cm^{-3}	ρ = 1.822 g cm^{-3}	ρ = 2.137 g cm^{-3}
Measurement limits	$-20 \le h \le 20$, $-21 \le k \le 21$, $-14 \le l \le 16$	$-19 \le h \le 10$, $-18 \le k \le 20$, $-15 \le l \le 15$	$-17 \le h < 17$; $-18 \le k < 18$, $-14 \le l < 13$
Theta range for data collection	3.8 to 58.8°	7.1 to 125.0°	3.8 to 52.0°
Wavelength	Mo-K_α (λ = 0.71073 Å)	Ga-K_α (λ = 1.34013 Å)	Mo-K_α (λ = 0.71073 Å)
Linear absorption coefficient	μ = 2.179 mm^{-1}	μ = 2.404 mm^{-1}	μ = 7.443 mm^{-1}
Number of reflections	10 461 (3758 independent)	16 119 (15 727 independent)	13 507 (independent 1752)
Refinement method	Full-matrix least-squares on F^2	Full-matrix least-squares on F^2	Full-matrix least-squares on F^2
Merging	R_{int} = 0.091	R_{int} = 0.012	R_{int} = 0.111
Number of parameters	167	167	157
Number of restrains	60[a]	14[a]	126[a]
Residual electron density	−0.88 to 0.63 $e^- \times 10^{-6}$ pm^{-3}	−0.68 to 0.87 $e^- \times 10^{-6}$ pm^{-3}	−2.41 to 0.78 $e^- \times 10^{-6}$ pm^{-3}
Figures of merit	R_1 ($I \ge 4\sigma_I$) = 0.035 R_1 (all data) = 0.049 wR_2 (all data) = 0.074 GooF = 1.021	R_1 ($I \ge 4\sigma_I$) = 0.028 R_1 (all data) = 0.030 wR_2 (all data) = 0.077 GooF = 1.079	R_1 ($I \ge 4\sigma_I$) = 0.043 R_1 (all data) = 0.066 wR_2 (all data) = 0.097 GooF = 0.937

[a] Restraints were used to address the disorder of the $[BMIm]^+$/$[BMPyr]^+$ cation and include fixed C–C and N–C distances (see deposited data with CSD 2041327–2041329†).

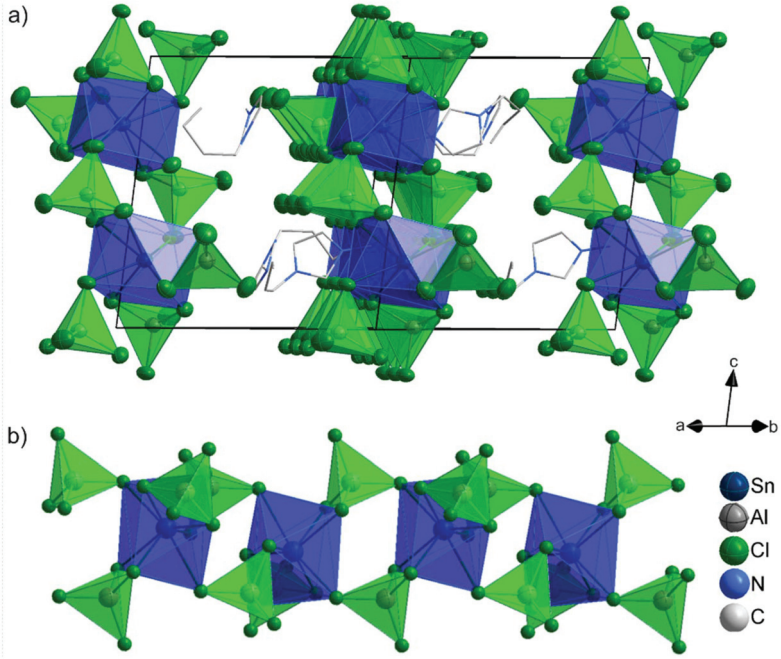

Fig. 2 Unit cell of the compounds **1–3** with [BMIm][Sn(AlCl$_4$)$_3$] (**1**) as example (a) as well as illustration of the infinite $^1_\infty$[Sn(AlCl$_4$)$_3$]$^{n-}$ chain (b) (polyhedra around Sn^{2+} in blue, [AlCl$_4$]$^-$ tetrahedra in green, [BMIm]$^+$ cation in grey with only one of two dislocated positions).

an eightfold coordination of Sn^{2+}/Pb^{2+} by chlorine (Fig. 2). All-in-all, this coordination leads to a distorted squared anti-prismatic polyhedron. Those two [AlCl$_4$]$^-$ tetrahedra that interlink neighboured Sn/Pb atoms in the $^1_\infty$[M(AlCl$_4$)$_3$]$^{n-}$ chain coordinate with two Cl atoms to one Sn/Pb atom and with one Cl atom to the neighboured Sn/Pb atom (Fig. 2). Hence, the [AlCl$_4$]$^-$ tetrahedra link Sn^{2+}/Pb^{2+} *via* one corner and one edge, whereas the fourth Cl atom remains non-coordinated. A similar linkage of Sn^{2+} with [AlCl$_4$]$^-$ was yet only reported for the metalorganic coordination compound [(η^6-C$_6$(CH$_3$)$_6$)Sn(AlCl$_4$)$_2$]$_2$·3C$_6$H$_6$, which contains a dimeric, molecular [Sn(AlCl$_4$)$_2$]$_2$ unit.[13] An additional [AlCl$_4$]$^-$ tetrahedron coordinated to Sn/Pb remains isolated and coordinates *via* two Cl atoms only to one Sn atom (Fig. 2). In the case of Pb^{2+}, examples with a comparable composition and coordination are rare as well. We have previously observed a chain-like connectivity *via* [AlCl$_4$]$^-$ in the carbonyl cluster compound [Pb{Mn(CO)$_5$}$_3$][AlCl$_4$].[14] Furthermore, metalorganic compounds such as [Pb(1,2-C$_6$H$_4$Me$_2$)$_2$(AlCl$_4$)$_2$] were reported.[15] Most recently, Ruck *et al.* observed a comparable coordination in Pb[AlCl$_4$]$_2$, however, with a bicapped trigonal prism as polyhedron around Pb^{2+}.[16]

The Sn–Cl distances in **1** and **2** range from 287.7(1) to 309.2 (1) pm (Table 2). Thereof, the shortest distances occur to non-bridging [AlCl$_4$]$^-$ tetrahedra (287.7(1), 289.8(1) pm), longer Sn–Cl distances are observed to corner-coordinating [AlCl$_4$]$^-$ tetrahedra (302.6(1), 304.0(1) pm) (Table 2 and Fig. 3). The longest Sn–Cl distances occur for one edge of the edge-coordinating [AlCl$_4$]$^-$ tetrahedra (294.8(1) and 306.7(1) pm in **1**; 296.3(1) and 309.2(1) pm in **2**). These distances are well in agreement with the literature. Thus, [(η^6-C$_6$(CH$_3$)$_6$)Sn(AlCl$_4$)$_2$]$_2$·3C$_6$H$_6$ as sole example containing [AlCl$_4$]$^-$-bridged Sn^{2+} exhibits Sn–Cl distances of 292.0–309.7 pm.[13] In [(η^6-C$_6$(CH$_3$)$_6$)Sn(AlCl$_4$)$_2$]$_2$·3C$_6$H$_6$, however, one Sn–Cl distance to [AlCl$_4$]$^-$ is significantly longer (332.2 pm) and consequently not considered as bridging edge by the authors.[13] In comparison to SnCl$_2$ (Sn–Cl: 260.4–330.2 pm), the distances in **1** and **2** are much closer together. For **3**, the Pb–Cl distances are 294.7(3)–304.5

Table 2 Sn–Cl and Pb–Cl distances in [BMIm][Sn(AlCl$_4$)$_3$] (**1**), [BMPyr][Sn(AlCl$_4$)$_3$] (**2**), and [BMIm][Pb(AlCl$_4$)$_3$] (**3**) in comparison to literature data

Compound	Coordination number	Bond length/pm
[BMIm][Sn(AlCl$_4$)$_3$] (**1**)	8	289.8(1), 294.8(1), 302.6(1), 306.7(1) (all 2×)
[BMPyr][Sn(AlCl$_4$)$_3$] (**2**)	8	287.7(1), 296.3(1), 304.0(1), 309.2(1) (all 2×)
SnCl$_2$ [18]	5	266.4, 278.2, 305.8, 321.9, 330.2
[(C$_6$(CH$_3$)$_6$)Sn(AlCl$_4$)$_2$]$_2$·3C$_6$H$_6$ [13]	5 + η^6(C$_6$H$_6$)	282.2, 304.3, 304.4, 309.7, 332.2
[BMIm][Pb(AlCl$_4$)$_3$] (**3**)	8	294.7(3), 298.2(3), 301.8(3), 304.5(3) (all 2×)
PbCl$_2$ [17]	9	279.5(1), 290.8(6) (2x), 303.5(2), 304.5(2) (2×), 308.9(6), 370.2(1) (2×)
Na[AlCl$_4$] [19]	4	212.9(1), 213.4(1), 214.0(1), 214.2(1)

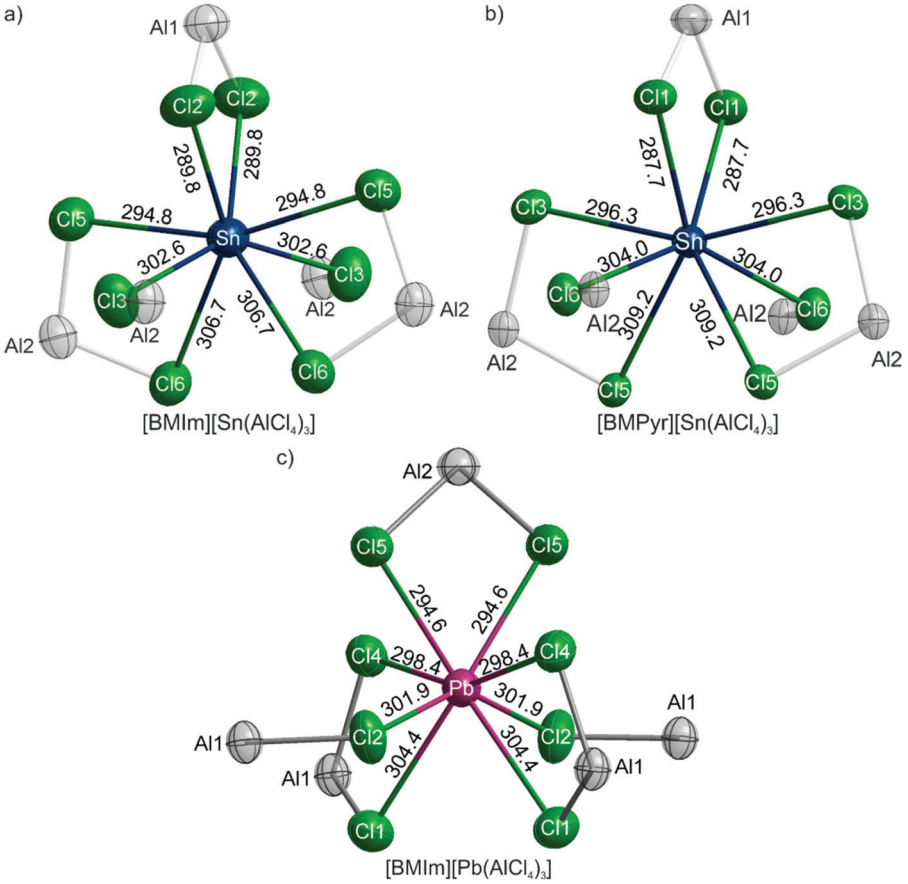

Fig. 3 Coordination of Sn^{2+} in [BMIm][$Sn(AlCl_4)_3$] (a) and [BMPyr][$Sn(AlCl_4)_3$] (b) as well as coordination of Pb^{2+} in [BMIm][$Pb(AlCl_4)_3$] (c).

(3) pm (Fig. 3). These values compare to those in $Pb(AlCl_4)_2$ (286.1–345.3 pm)[16] and $PbCl_2$ (279.5–308.9 pm) (Table 2).[17] The narrow distribution range of the Sn–Cl and Pb–Cl distances in comparison to the reference compounds also indicates the lone-pair of Sn^{2+}/Pb^{2+} to be stereochemically non-active.

As discussed before, Sn^{2+} and Pb^{2+} are coordinated in a squared anti-prismatic manner. The Cl···Cl···Cl angles in the squared plane are 87.1(1) and 93.8(1)° (**1**), 86.7(1) and 92.6(1)° (**2**), as well as 87.0 and 93.8° (**3**). The Cl···Cl distances range from 333.2(1) to 392.2(1) pm (**1**), 335.1(1) to 383.3(1) pm (**2**), and 334.5(4) to 398.3(4) pm (**3**). The $[AlCl_4]^-$ tetrahedra are slightly distorted for all title compounds and exhibit Cl–Al–Cl angles of 101.1(1)–113.6(1)° as well as Al–Cl distances of 207.9 (1)–217.4(1) pm. Terminal Cl atoms show shorter distances than bridging Cl atoms. All these distances are in the expected range (*e.g.*, Na[$AlCl_4$]: 212.9(1)–214.2(1) pm).[19] Beside the infinite $^1_\infty[M(AlCl_4)_3]^{n-}$ chains, the structure and connectivity of both cations $[BMIm]^+$ and $[PMPyr]^+$ are as expected. For the $[BMIm]^+$ cations in **1** and **3**, two more-or-less rotated (180°) sites are observed (ESI: Fig. S3†). This situation was tackled by split positions for all atoms of the $[BMIm]^+$ cation with a probability of finding of 50% for each position.

In addition to the crystal structure analysis, the purity and composition of all title compounds were examined by Fourier-transform infrared spectroscopy (FT-IR) and thermal analysis, including differential thermal analysis (DTA) and thermogravimetry (TG). FT-IR spectra predominately show vibrations

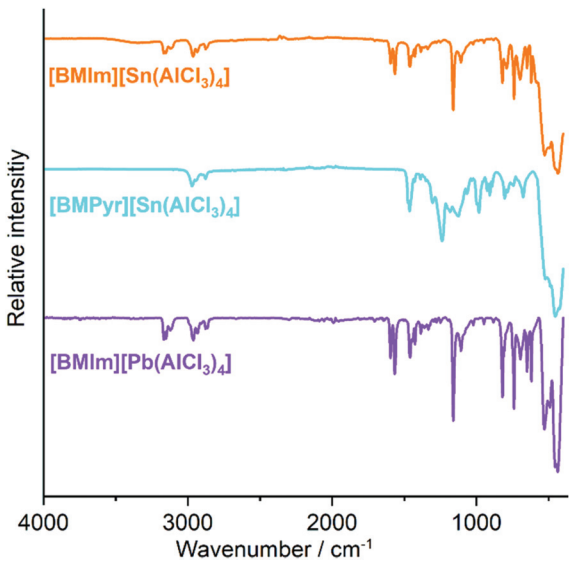

Fig. 4 Infrared spectra of [BMIm][$Sn(AlCl_4)_3$] (**1**), [BMPyr][$Sn(AlCl_4)_3$] (**2**) and [BMIm][$Pb(AlCl_4)_3$] (**3**).

related to the $[BMIm]^+$/$[BMPyr]^+$ cations (Fig. 4), including ν(C–H) at 3300–2800 cm^{-1}, ν(C=N) at 1650–1600 cm^{-1}, as well as the fingerprint area (1500–500 cm^{-1}).[20] Furthermore, vibrations of the $[AlCl_4]^-$ tetrahedra (ν(Al–Cl)) are visible below 600 cm^{-1} (Fig. 4). Finally, it should be noticed that no ν(O–H) vibrations are observed (3600–3000 cm^{-1}), which indicates the absence of any moisture. Taking the similar composition and structure into account, the thermal behaviour of the title compounds is surprisingly different (Fig. 5). Endothermic peaks in the DTA analysis, first of all, indicate the melting points of the tin-containing compounds at 91 (**1**) and 108 °C (**2**). For **3**, a melting point is not observed (except for the endothermal peak at 500 °C indicating the melting point of $PbCl_2$). TG exhibits a two-step decomposition for **1** and **3**, whereas one-step decomposition is observed for **2**. Moreover, **2** is highly stable and starts decomposing only above 400 °C, which is even more remarkable since the compound is already in the liquid state. For all compounds, low quantities of a deep black residue were observed after TG analysis, which was finely distributed all over the crucible surface. In sum, the thermal decomposition can be rationalized based on a total decomposition of the $[BMIm]^+$/$[BMPyr]^+$ cation, evaporation of all Al_2Cl_6, and elemental Sn and Pb as solid residue.

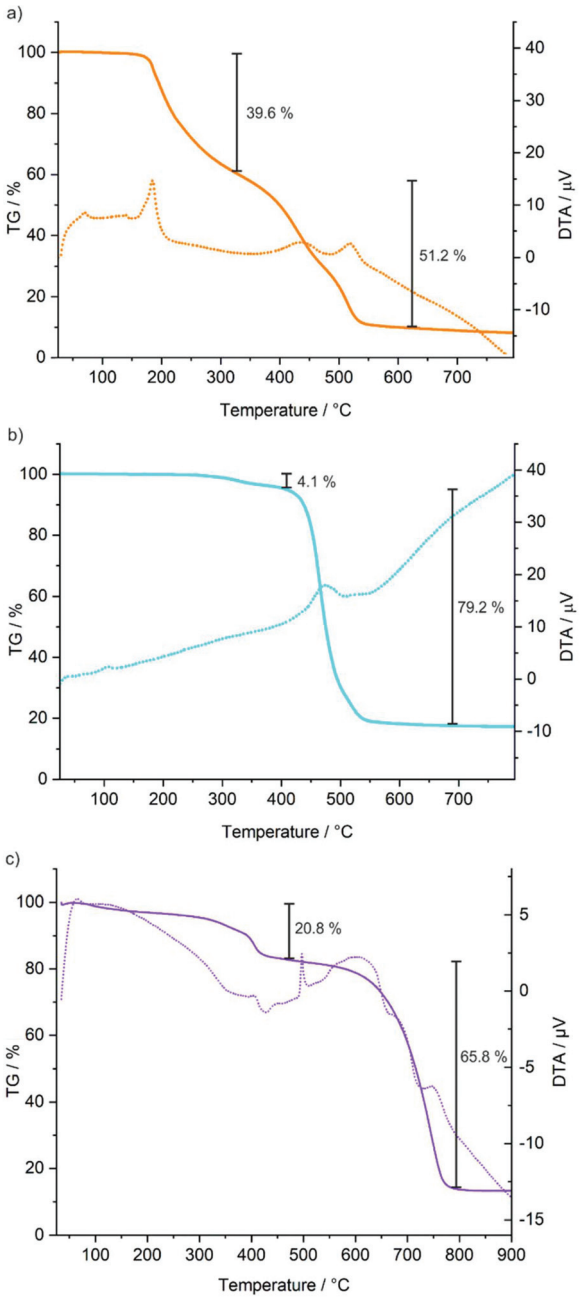

Fig. 5 Thermal analysis with thermogravimetry (TG) and differential thermal analysis (DTA) of [BMIm][Sn($AlCl_4$)$_3$] (a) and [BMPyr][Sn($AlCl_4$)$_3$] (b) as well as of [BMIm][Pb($AlCl_4$)$_3$] (c).

Photoluminescence properties

Sn^{2+} as well as Pb^{2+} are well-known for their luminescence originating from s–p transitions.[21] These transitions are parity-allowed and can be very efficient. Thus, they are also used in commercial phosphors. Selected examples comprise Pb^{2+}-doped UV-emitting phosphors such as $CaSiO_3$:Pb^{2+} or the Sn^{2+}-doped fluorescent-lamp phosphors $Ba_2Li_2Si_2O_7$:Sn^{2+}, $Ca_3(PO_4)_2$:Sn^{2+} and $Ca_5(PO_4)_3F$:Sn^{2+} (Table 3).[22,23] Herein, Sn^{2+}/Pb^{2+} as a luminescent center is present as a dopant in a non-luminescent host lattice with a typical concentration range of 5–10 mol%.[21,22] This concentration range is normally essential to avoid concentration quenching, which otherwise results in a drastic reduction of the emission efficiency due to continuous energy exchange between directly neighboured luminescent centers.[21] For conventional phosphors, moreover, metal oxides are used most often as host lattice, since they only exhibit low-energy lattice vibrations at room temperature, so that vibrational loss processes are low as well. In addition to these

Table 3 Photoluminescence properties of [BMIm][Sn($AlCl_4$)$_3$] (**1**), [BMPyr][Sn($AlCl_4$)$_3$] (**2**), and [BMIm][Pb($AlCl_4$)$_3$] (**3**) in comparison to literature data on Sn^{2+}-containing compounds

Compound	Maximum of excitation/nm	Maximum of emission/nm	Quantum yield/%
[BMIm][Sn($AlCl_4$)$_3$] (**1**)	291	448	51
[BMPyr][Sn($AlCl_4$)$_3$] (**2**)	296	453	76
[BMIm][Pb($AlCl_4$)$_3$] (**3**)	350	416, 571	2
$Ba_2Li_2Si_2O_7$:Sn^{2+} (5 mol%)[22]	254	429	60–70
$Ca_3(PO_4)_2$:Sn^{2+} (5 mol%)[23a]	254	646	80–90
$Ca_5(PO_4)_3F$:Sn^{2+} (10 mol%)[23b]	254	413	80–90
$[C_6N_2H_{16}Cl]_2[SnCl_6]$[29a]	365	450	8
Cs_4SnBr_6 [29b]	365	534	21
$[C_6H_{13}NH_3]_2[SnBr_4]$[30]	335	618	35
$[C_8H_{17}NH_3]_2[SnBr_4]$[30]	344	610	82
$[C_{12}H_{25}NH_3]_2[SnBr_4]$[30]	338	603	60
$[C_{18}H_{35}NH_3]_2[SnBr_4]$[30]	339	623	52
0D-[(PEA)$_4$SnBr$_6$][(PEA)Br]·(CCl_2H_2)$_2$ [26]	304	566	90
2D-[(PEA)$_4$SnBr$_6$][(PEA)Br]·(CCl_2H_2)$_2$ [26]	304	566	0.1
$[Bmpip]_2[SnBr_4]$[25a]	405	665	75
2D-$[C_8H_{17}NH_3]_2[SnI_4]$[25b]	340	670	95

PEA: phenylethylammonium; Bmpip: 1-butyl-1-methyl-piperidinium.

conventional phosphors, organic–inorganic hybrid tin/lead halides have only entered the literature since 2019 in the wake of the discovery of the methylammonium lead iodide perovskite as a promising new solar absorber.[24] Here, efficient fluorescence has been reported, particularly for hybrid tin/lead bromides and iodides (Table 3). However, due to the small bandgap, excitation and/or emission occur *via* valence-band-to-conduction-band transitions (especially for the respective iodides), which superimpose the s–p transitions of Sn^{2+}/Pb^{2+}.[24,25] Such semiconductor-based luminescence leads to high quantum yields of nanoparticles. For instance, $[(PEA)_4SnBr_6][(PEA)Br]\cdot(CCl_2H_2)_2$ exhibits excellent efficiency as a zero-dimensional quantum dot (90%),[26] whereas two-dimensional infinite layers of the compound have only a marginal quantum yield (0.1%) (Table 3).

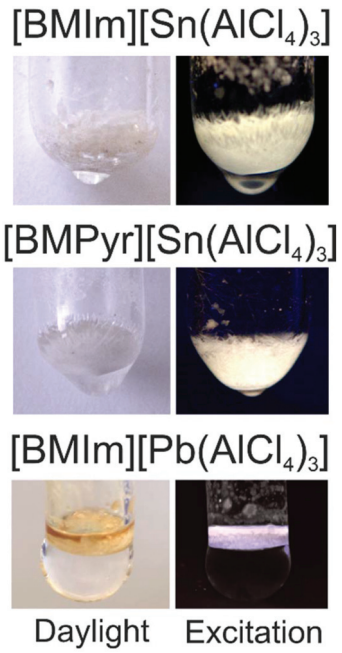

Fig. 6 Photos showing $[BMIm][Sn(AlCl_4)_3]$, $[BMPyr][Sn(AlCl_4)_3]$, and $[BMIm][Pb(AlCl_4)_3]$ in daylight and under UV-excitation.

In regard of the aforementioned considerations, the colourless title compounds **1–3** represent wide-band-gap materials and contain Sn^{2+}/Pb^{2+} in molar quantities. Nevertheless, they show considerable yellowish to white emission, which is clearly visible for the naked eye under UV-excitation (Fig. 6). Excitation and emission spectra indicate strong absorption at 280–320 nm and intense emission at 400–550 nm for $[BMIm][Sn(AlCl_4)_3]$ and $[BMPyr][Sn(AlCl_4)_3]$ (Table 3 and Fig. 7). $[BMIm][Pb(AlCl_4)_3]$ can be excited at 320–550 nm and emits at 400–700 nm (Table 3 and Fig. 7). The observed decay times are in a range of 1×10^{-7} to 1.0×10^{-6} s, which is expected for parity-allowed s–p transitions of Sn^{2+}/Pb^{2+}. The broad peak widths for excitation and especially for emission are also expected for s–p transitions[21] and can be assigned to a $^1S_0$ ground state of the s^2 electrons. The excited state is represented by $^3P_0$, $^3P_1$, $^3P_2$ and $^1P_1$ states with $^3P_1 \rightarrow {}^1S_0$ as preferred relaxation to the ground state.[27] For the heavy Pb^{2+}, $^3P_0 \rightarrow {}^1S_0$ transition is also possible due to spin–orbit coupling and explains the double-band structure of excitation and emission as well as the very broad emission in the case of $[BMIm][Pb(AlCl_4)_3]$.[21]

The efficiency of the photoluminescence processes was quantified by determining the absolute quantum yield following the method given by Friend *et al.*[28] Whereas the quantum yield of $[BMIm][Pb(AlCl_4)_3]$ is low (2%), the quantum yields of $[BMIm][Sn(AlCl_4)_3]$ and $[BMPyr][Sn(AlCl_4)_3]$ are surprisingly high with values of 51% and 76%, respectively (Table 3). Comparing the quantum yield of the Sn^{2+}-containing compounds with literature data, it is first noticeable that there are only few examples with quantum yields around 80% even among the long-optimized conventional Sn^{2+}-doped phosphors. Here, $Ba_2Li_2Si_2O_7:Sn^{2+}$, $Ca_3(PO_4)_2:Sn^{2+}$ or $Ca_5(PO_4)_3F$:

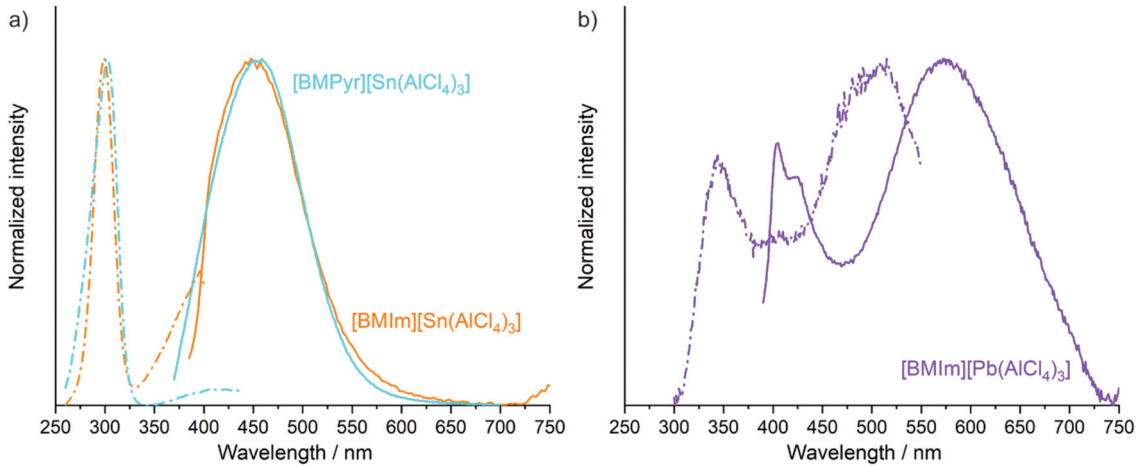

Fig. 7 Photoluminescence spectra of $[BMIm][Sn(AlCl_4)_3]$ and $[BMPyr][Sn(AlCl_4)_3]$ (a) as well as of $[BMIm][Pb(AlCl_4)_3]$ (b) (dashed line: excitation; solid line: emission).

Sn^{2+} belong to those with the highest quantum yield of Sn^{2+}-doped phosphors (Table 3).[22,23] For ionic organic–inorganic hybrid tin chlorides and bromides with s–p-based luminescence of Sn^{2+} (*e.g.* $[C_6N_2H_{16}Cl]_2[SnCl_6]$, Cs_4SnBr_6),[29] the quantum yields are so far also significantly lower than for the title compounds **1** and **2**. In a seminal work, Deng *et al.* recently correlated the quantum yield of hybrid tin bromides $[C_nH_{2n+1}NH_3]_2[SnBr_4]$ (n = 6–18) with the length of the alkyl chain and the distance between the Sn^{2+} centers and observed a maximum for n = 8 with a quantum yield of 82% (Table 3).[30] This points to the necessity of large distances between the luminescent Sn^{2+} centers to avoid concentration quenching. With increasing length of the alkyl chain, however, the influence of vibrational loss processes related to the organic cation is increased and reduces the quantum yield. $[BMIm][Sn(AlCl_4)_3]$ and $[BMPyr][Sn(AlCl_4)_3]$ in this regard are unique as they – to the best of our knowledge – exhibit the highest quantum yield known for s–p-based luminescence of Sn^{2+}. This finding can be ascribed to the rigid coordination of Sn^{2+} in the $^1_\infty[Sn(AlCl_4)_3]^{n-}$ chain and the large distance between the luminescent centers ($Sn^{2+}\cdots Sn^{2+}$: 644.2(1) pm (**1**) and 647.1(1) pm (**2**)) with the $[AlCl_4]^-$ tetrahedra serving as spacers. Especially, $[BMPyr][Sn(AlCl_4)_3]$ is obviously a good compromise between a large distance and a rigid coordination of the luminescent centers.

Conclusion

The chloridoaluminates $[BMIm][Sn(AlCl_4)_3]$ (**1**) ([BMIm]: 1-butyl-3-methylimidazolium) and $[BMPyr][Sn(AlCl_4)_3]$ (**2**) ([BMPyr]: 1-butyl-1-methyl-pyrrolidinium), and $[BMIm][Pb(AlCl_4)_3]$ (**3**) are obtained by reaction of $SnCl_2$/$PbCl_2$ in a Lewis-acidic ionic liquid based on mixtures of [BMIm]Cl or [BMPyr]Cl and $AlCl_3$. The crystal structures of the title compounds are characterized by a novel infinite $^1_\infty[M(AlCl_4)_3]^{n-}$ chain (M: Sn, Pb) that is separated by the voluminous $[BMIm]^+$/$[BMPyr]^+$ cations. Herein, the central Sn^{2+}/Pb^{2+} is coordinated by chlorine in the form of distorted squared anti-prismatic polyhedra. Surprisingly, all compounds show emission of white to yellowish light. Although Sn^{2+}/Pb^{2+} are well-known as luminescent centers, efficient luminescence of ionic, wide-band-gap compounds containing the luminescent center as regular lattice constituents (instead of doping) is unusual. In this regard, $[BMIm][Sn(AlCl_4)_3]$ and $[BMPyr][Sn(AlCl_4)_3]$ with 51 and 76% show surprisingly high quantum yields, which belong to the highest values observed for s–p transitions on Sn^{2+}. This finding can be ascribed to the rigid coordination of Sn^{2+} in the $^1_\infty[Sn(AlCl_4)_3]^{n-}$ chains and the large distance between the $[AlCl_4]^-$-bridged luminescent Sn^{2+} centers.

Experimental section

Synthesis of compounds

General. All reactions and sample handling were carried out under dried argon atmosphere using standard Schlenk techniques or glove boxes (MBraun Unilab, $c(O_2, H_2O)$ < 0.1 ppm). Reactions were performed in Schlenk flasks and glass ampoules that were evacuated ($p < 10^{-3}$ mbar), heated, and flashed with argon three times before use. The starting materials $SnCl_2$ (99.99%, ABCR), $AlCl_3$ (99.99%, Sigma-Aldrich) and $PbCl_2$ (99%, VWR) were used as received. [BMIm]Cl (99%, Iolitec) and [BMPyr]Cl (99%, Iolitec) were dried under reduced pressure (10^{-3} mbar) at 130 °C for 48 h.

$[BMIm][Sn(AlCl_4)_3]$ (1). 100 mg (1 eq., 0.527 mmol) of $SnCl_2$, 92.1 mg (1 eq., 0.527 mmol) of [BMIm]Cl and 211.0 mg (3 eq., 1.582 mmol) of $AlCl_3$ were heated under argon in a sealed glass ampoule for 12 hours at 80 °C. After cooling to room temperature with a rate of 1 K h^{-1}, **1** was obtained in the form of colorless needles in a slightly yellowish ionic liquid with a yield of about 75%. **1** is very sensitive to moisture and hydrolyses in air within seconds. Hence, **1** needs to be strictly handled under inert conditions.

$[BMPyr][Sn(AlCl_4)_3]$ (2). 100 mg (1 eq., 0.527 mmol) of $SnCl_2$, 93.7 mg (1 eq., 0.527 mmol) of [BMPyr]Cl and 211.0 mg (3 eq., 1.582 mmol) of $AlCl_3$ were heated under argon in a sealed glass ampoule for 12 hours at 100 °C. After cooling to room temperature with a rate of 1 K h^{-1}, **2** was obtained as colorless needles in a slightly yellowish ionic liquid with a yield of about 80%. **2** is very sensitive to moisture and hydrolyses in air within seconds. Hence, **2** needs to be strictly handled under inert conditions.

$[BMIm][Pb(AlCl_4)_3]$ (3). 78 mg (1 eq., 0.283 mmol) of $PbCl_2$, 50 mg (1 eq., 0.283 mmol) of [BMIm]Cl and 113 mg (3 eq., 0.849 mmol) of $AlCl_3$ were heated under argon in a sealed glass ampoule for 96 h at 70 °C. Thereafter, the ampoule was cooled to room temperature with a rate of 1 K h^{-1}. Thereafter, **3** was obtained as colorless rhombohedra crystals in a slightly yellowish ionic liquid with a yield of about 64%. The crystals are highly sensitive to moisture and hydrolyse in air within seconds. Hence, **3** needs to be strictly handled under inert conditions.

Analytical equipment

Single crystal structure analysis. Suitable single crystals of all title compounds were manually selected, covered by inert-oil (perfluoropolyalkylether, ABCR), and deposited on a micro gripper (MiTeGen). Data collection for **1** and **3** was performed at 213 K on an IPDS II image-plate diffractometer (Stoe, Darmstadt) using Mo-K_α radiation (λ = 0.71073 Å, graphite monochromator). Data collection for **2**, which formed significantly smaller crystals than **1** and **3**, was performed at 180 K on an Stoe StadiVari Diffractometer with Euler geometry (Stoe, Darmstadt) using Ga-K_α radiation (λ = 1.34013 Å, graded multilayer mirror as the monochromator). Data reduction and multi-scan absorption correction were conducted using the X-AREA software package and STOE LANA (version 1.75).[31] Space group determinations based on systematic absences of reflections were performed by XPREP. Using Olex2,[32] all crystal structures were solved with the ShelXS structure solution program using Direct Methods and refined with the ShelXL refinement package, using least squares minimization.[33] All non-hydrogen atoms were refined anisotropically. The posi-

tions of the hydrogen atoms could not be located *via* Fourier refinement and were modelled by idealized C–H bonds. Detailed information related to crystallographic data and structure refinements are listed in Table 1. DIAMOND was used for all illustrations.[34] Refinements were validated with PLATON.[35] Further details of the crystal structure investigations may be obtained from the joint CCDC/FIZ Karlsruhe deposition service on quoting the depository number CSD 2041327–2041329.†

Fourier-transform infrared (FT-IR) spectra were recorded on a Bruker Vertex 70 FT-IR spectrometer (Bruker). The samples were measured as pellets in KBr. Thus, 300 mg of dried KBr and 0.5–1.0 mg of the sample were carefully pestled and pressed to a thin pellet.

Thermogravimetry (TG) was carried out with a Netzsch STA 449 F3 Jupiter device, using α-Al_2O_3 as crucible material and reference. Buoyancy effects were corrected by baseline subtraction of a blank measurement. The samples were measured under dried nitrogen up to 800 °C with a heating rate of 10 K min^{-1}. The reaction gas was analyzed *via* IR-coupling by a Bruker Vertex 70 FT-IR spectrometer (Bruker). The Netzsch software PROTEUS Thermal Analysis (Version 5.2.1) was used for graphical illustration.

Fluorescence spectroscopy. Excitation and emission spectra were recorded using a photoluminescence spectrometer Horiba Jobin Yvon Spex Fluorolog 3, equipped with a 450 W Xenon lamp, double monochromator for excitation and emission, an integrating sphere (Ulbricht sphere) and a photomultiplier as the detector. The determination of the quantum yield was performed according to Friend *et al.*[28] First of all, the diffuse reflection of the sample was determined under excitation conditions. Thereafter, the emission was measured at this excitation wavelength. Integration over the reflected and emitted photons by use of the Ulbricht sphere results in the absolute quantum yield. Corrections were made regarding the spectral power of the excitation source, the reflection behavior of the Ulbricht sphere and the sensitivity of the detector.

Conflicts of interest

There are no conflicts to declare.

Acknowledgements

The authors thank the Deutsche Forschungsgemeinschaft (DFG) for funding in the Priority Program SPP1708 "*Material synthesis near room temperature*". Moreover, we acknowledge the Karlsruhe Nano Micro Facility (KNMF) and Prof. Dr D. Fenske and Dr A. Eichhöfer for data collection on a Stoe StadiVari diffractometer with Ga-metal-jet source.

References

1 Reviews: (*a*) A. R. West, *Solid State Chemistry and its Applications*, Wiley, Chichester, 2014; (*b*) J. D. Corbett, *J. Alloys Compd.*, 2006, **418**, 1–20; (*c*) G. Meyer, *Prog. Solid State Chem.*, 1982, **14**, 141–219.
2 C. Feldmann, *Angew. Chem., Int. Ed.*, 2013, **52**, 7610–7611.
3 Review: C. R. Boston, *Adv. Molten Salt Chem.*, 1971, **1**, 129–163.
4 Review: (*a*) E. Ahmed and M. Ruck, *Dalton Trans.*, 2011, **40**, 9347–9357; (*b*) D. Freudenmann, S. Wolf, M. Wolff and C. Feldmann, *Angew. Chem., Int. Ed.*, 2011, **50**, 11050–11060; (*c*) J. Dupont, *Acc. Chem. Res.*, 2011, **44**, 1223–1231.
5 P. Wasserscheid and W. Keim, *Angew. Chem., Int. Ed.*, 2000, **39**, 3772–3789.
6 M. Knies, M. Kaiser, A. Isaeva, U. Mueller, Th. Doert and M. Ruck, *Chem. – Eur. J.*, 2018, **24**, 127–132.
7 S. Wolf, W. Klopper and C. Feldmann, *Chem. Commun.*, 2018, **54**, 1217–1220.
8 E. Ahmed, A. Isaeva, A. Fiedler, M. Haft and M. Ruck, *Chem. – Eur. J.*, 2011, **17**, 6847–6852.
9 P. Simon, Z. Tang, W. Carrillo-Cabrera, K. Chiong, B. Bohme, M. Baitinger, H. Lichte, Y. Grin and A. M. Guloy, *J. Am. Chem. Soc.*, 2011, **133**, 7596–7601.
10 K. Biswas, Q. Zhang, I. Chung, J. H. Song, J. Androulakis, A. J. Freeman and M. G. Kanatzidis, *J. Am. Chem. Soc.*, 2010, **132**, 14760–14762.
11 C. E. Runyan and T. Hughbanks, *J. Am. Chem. Soc.*, 1994, **116**, 7909–7910.
12 P. Wasserscheid and T. Welton, *Ionic Liquids in Synthesis*, Wiley-VCH, Weinheim, 2007.
13 H. Schmidbaur, T. Probst, O. Steigelmann and G. Müller, *Z. Naturforsch.*, 1989, **44b**, 1175–1178.
14 S. Wolf, D. Fenske, W. Klopper and C. Feldmann, *Dalton Trans.*, 2019, **48**, 4696–4701.
15 (*a*) W. Frank and F.-G. Wittmer, *Chem. Ber.*, 1997, **130**, 1731–1732; (*b*) T. Auel and E. L. Amma, *J. Am. Chem. Soc.*, 1968, **90**, 5941–5942.
16 M. Knies, M. Lê Anh, U. Keßler and M. Ruck, *Z. Naturforsch., B: J. Chem. Sci.*, 2020, **75**, 117–123.
17 R. L. Sass, E. B. Brackett and T. E. Brackett, *J. Phys. Chem.*, 1963, **67**, 2863–2864.
18 J. M. van den Berg, *Acta Crystallogr.*, 1961, **14**, 1002–1003.
19 (*a*) G. Mairesse, P. Barbier and J.-P. Wignacourt, *Acta Crystallogr., Sect. B: Struct. Crystallogr. Cryst. Chem.*, 1979, **35**, 1573–1580; (*b*) W. Scheinert and A. Weiss, *Z. Naturforsch., A: Phys. Sci.*, 1976, **31**, 1354–1369.
20 (*a*) Y. Jeon, J. Sung, C. Seo, H. Lim, H. Cheong, M. Kang, B. Moon, Y. Ouchi and D. Kim, *J. Phys. Chem. B*, 2008, **112**, 4735–4740; (*b*) T. Liu, Y. Danten, J. Grondina and R. Vilarb, *J. Raman Spectrosc.*, 2016, **47**, 449–456.
21 G. Blasse and B. C. Grabmaier, *Luminescent Materials*, Springer, Berlin, 1994.
22 W. M. Yen, S. Shionoya and H. Yamamoto, *Phosphor Handbook*, CRC Press, Boca Raton, 2006.
23 (*a*) E. R. Kreidler, *J. Electrochem. Soc.*, 1971, **118**, 923–929; (*b*) H. J. Jenkins, A. H. McKeag and P. W. Ranby, *J. Electrochem. Soc.*, 1949, **96**, 1–12.
24 (*a*) S. Lee, C. Zhou, J. Neu, D. Beery, A. Arcidiacono, M. Chaaban, H. Lin, A. Gaiser, B. Chen, T. E. Albrecht-Schmitt, T. Siegrist and B. Ma, *Chem. Mater.*, 2020, **32**, 374–

380; (*b*) Q. Zhang, Y. Ji, Z. Chen, D. Vella, X. Wang, Q.-H. Xu, Y. Li and G. Eda, *J. Phys. Chem. Lett.*, 2019, **10**, 2869–2873; (*c*) C. Wu, T. Wu, Y. Yang, J. A. McLeod, Y. Wang, Y. Zou, T. Zhai, J. Li, M. Ban, T. Song, X. Gao, S. Duhm, H. Sirringhaus and B. Sun, *ACS Nano*, 2019, **13**, 1645–1654; (*d*) H. Zhu, Y. Fu, F. Meng, X. Wu, Z. Gong, Q. Ding, M. V. Gustafsson, M. T. Trinh, S. Jin and X.-Y. Zhu, *Nat. Mater.*, 2015, **14**, 636–643.

25 (*a*) V. Morad, Y. Shynkarenko, S. Yakunin, A. Brumberg, R. D. Schaller and M. V. Kovalenko, *J. Am. Chem. Soc.*, 2019, **141**, 9764–9768; (*b*) A. Wang, Y. Guo, Z. Zhou, X. Niu, Y. Wang, F. Muhammad, H. Li, T. Zhang, J. Wang, S. Nie and Z. Deng, *Chem. Sci.*, 2019, **10**, 4573–4579.

26 L.-J. Xu, H. Lin, S. Lee, C. Zhou, M. Worku, M. Chaaban, Q. He, A. Plaviak, X. Lin, B. Chen, M.-H. Du and B. Ma, *Chem. Mater.*, 2020, **32**, 4692–4698.

27 B. Gaveau, E. Mihokova, M. Nikl, K. Polak and L. S. Schulman, *Phys. Rev. B: Condens. Matter Mater. Phys.*, 1998, **58**, 6938–6943.

28 J. C. de Mello, H. F. Wittmann and R. H. Friend, *Adv. Mater.*, 1997, **9**, 230–232.

29 (*a*) G. Song, M. Li, Y. Yang, F. Liang, Q. Huang, X. Liu, P. Gong, Z. Xia and Z. Lin, *J. Phys. Chem. Lett.*, 2020, **11**, 1808–1813; (*b*) L. Tan, W. Wang, Q. Li, Z. Luo, C. Zou, M. Tang, Z. Min;, L. Zhang, J. He and Z. Quan, *Chem. Commun.*, 2020, **56**, 387–390.

30 Y. Liu, A. Wang, J. Wu, C. Wang, Z. Li, G. Hu, S. Sui, J.-X. She, W. Meng, W. Li and Z. Deng, *Mater. Adv.*, 2021, **2**, 1320–1327.

31 J. Koziskova, F. Hahn, J. Richter and J. Kozisek, *Acta Chim. Slov.*, 2016, **9**, 136–140.

32 O. V. Dolomanov, L. J. Bourhis, R. J. Gildea, J. A. K. Howard and H. Puschmann, *J. Appl. Crystallogr.*, 2009, **42**, 339–341.

33 (*a*) G. M. Sheldrick, *Acta Crystallogr., Sect. A: Found. Crystallogr.*, 2008, **64**, 112–122; (*b*) G. M. Sheldrick, *Acta Crystallogr., Sect. C: Struct. Chem.*, 2015, **71**, 3–8.

34 *DIAMOND Version 4.2.2 – Crystal and Molecular Structure Visualization*, Crystal Impact GbR, Bonn, 2016.

35 (*a*) A. L. Spek, *Acta Crystallogr., Sect. D: Biol. Crystallogr.*, 2009, **65**, 148–155; (*b*) A. L. Spek, *Acta Crystallogr., Sect. C: Struct. Chem.*, 2015, **71**, 9–18.